11th International Symposium on Turbulence and Shear Flow Phenomena (TSFP11)
Southampton, UK, July 30 to August 2, 2019

EXPERIMENTAL INVESTIGATION INTO THE INFLUENCE OF TRAILING EDGE GEOMETRY AND PITCHING AMPLITUDE ON THE SPANWISE CIRCULATION SHED BY BIO-INSPIRED PITCHING PANELS

Justin T. King
Department of Mechanical and Aerospace Engineering
Syracuse University
263 Link Hall Syracuse, NY 13244, USA
jtking@syr.edu

Melissa A. Green
Department of Mechanical and Aerospace Engineering
Syracuse University
263 Link Hall Syracuse, NY 13244, USA
greenma@syr.edu

INTRODUCTION

Recently, engineers have turned to the study of swimming and flying animals to provide insight into the design of vehicles that move through air or water (Triantafyllou *et al.* (2004); Bandyopadhyay (2005); Shang *et al.* (2009)). For certain swimming animals, thrust is generated primarily by a caudal fin or fluke that is located at the posterior extreme of the swimmer (Lighthill (1969); Fierstine (1965)). These propulsive surfaces can display a wide range of planform geometries, including those with straight, forked, or pointed trailing edge shapes (Lighthill (1969); Lauder (2000)). In the current work, the wakes produced by bio-inspired propulsors are examined through an investigation of the spanwise circulation shed by pitching panels with a swept leading edge. Multiple panel geometries, based upon a trapezoidal planform but with different trailing edge shapes, were chosen as rudimentary approximations of the caudal fin and fluke shapes found in a variety of aquatic swimmers.

The circulation shed by panels and foils has been studied in previous experimental work. Buchholz *et al.* (2011) explored the total, positive spanwise circulation shed from the trailing edge of a series of pitching rectangular panels. Using kinematic and geometric arguments, a scaling relationship of the non-dimensional spanwise circulation was developed that produced an approximately constant value across a range of Strouhal (St) numbers, geometric parameters, and kinematic parameters. The three-dimensional wake of a trapezoidal plate rotated from rest about its leading edge at a 90° angle of attack was studied by DeVoria & Ringuette (2012). Calculations of total spanwise circulation and the spanwise circulation of the primary trailing edge vortex were used to determine the effects of velocity program on the saturation of vortices shed from the trailing edge of the rotating panel. Saturation was defined as an existence of an upper limit in the strength, as related by circulation, that a vortex ring can ultimately attain. It was found that pressure gradients acting along the chord of the panel strongly affected the saturation of spanwise vortices shed from the trailing edge. The formation and circulation of leading edge vortices created by pitching and heaving foils and panels has also been investigated experimentally (Milano & Gharib (2005); Rival *et al.* (2009); Carr *et al.* (2013, 2015)).

The saturation of vortex rings has been identified through the use of a "formation number" introduced for the study of piston-generated vortex rings by Gharib *et al.* (1998). The formation number is the specific value of the non-dimensional formation time at which a vortex ring becomes saturated and is no longer able to accept additional vorticity. It was speculated that the observed formation number of approximately 4 was universal among piston-generated vortex rings. The concept of formation time and formation number has also been applied to bio-inspired propulsion and oscillating propulsors (Dabiri (2009); Rival *et al.* (2009); Milano & Gharib (2005)). In these studies, the formation number of the oscillating propulsors was also observed to be approximately 4, although different formulations among the studies were used for the definition of the velocity scalings used for the calculation of formation time. In other experimental work, formation numbers of much less than 4 have been found to occur for trapezoidal plates rotated from rest in a stationary fluid by DeVoria & Ringuette (2012). In that work, the authors commented upon the difference between oscillating propulsive mechanisms that rely on the development of jet-like fluid momentum, e.g. fish-like swimming, versus those that rely on the attachment and shedding of a vortex, e.g. the leading edge vortex of a drag-based flyer. Due to the differences in propulsive mechanisms, it was suggested that for fish-like swimming the formation parameter may have to be redefined to provide more reliable estimates of saturation.

The current work draws upon results obtained from multiple planes of stereoscopic particle image velocimetry

to explore the dimensional spanwise circulation shed from the trailing edge of trapezoidal pitching panels with different trailing edge geometries that were pitched about their leading edge. The effects of varying Strouhal number on circulation are also analyzed through changes in pitching amplitude. Furthermore, the presence of vortex saturation in the wake is investigated and the relationship between spanwise position and spanwise circulation is explored.

EXPERIMENTAL SETUP AND CALCULATION METHODS

All experiments were performed in a recirculating water tunnel that used a constant free-stream speed of 80 mm/s. Stereoscopic particle image velocimetry (PIV) was used to capture three-component velocity vectors in the flow field within 27 chordwise-oriented planes. The spanwise spacing between the planes was constant and the planes were positioned from the plane of symmetry at the midspan of the panel to slightly below its lower spanwise tip. A total of five different panel geometries were sinusoidally pitched about their leading edge at a frequency of 1 Hz. Furthermore, each panel was pitched with five different angular pitching amplitudes, $\phi_{\max}$, providing a Strouhal number range of $0.09 \leq St \leq 0.66$. In the current work, the Strouhal number is defined as $St = f\bar{A}/U$, where f is the pitching frequency, $\bar{A}$ is the average value of the peak-to-peak trailing edge excursion across the span of the panel, and U is the free-stream speed. For all panel geometries besides Panel 3, i.e. the panel with a straight trailing edge, the peak-to-peak trailing edge excursion is a function of spanwise location due to the trailing edge geometry. Accordingly, the average value of trailing edge amplitude taken across the entire span of the panel is used for the definition of St. By defining St in such a manner, variations in trailing edge geometry among panels pitching with the same maximum trailing edge amplitude, e.g. among Panels 1-3 at the same value of $\phi_{\max}$, are captured so that a panel with a more forked trailing edge has a lower St. The St range studied in the current work was chosen to match the range used by swimming fish and cetaceans (Triantafyllou *et al.* (1993)).

The details of the experimental setup and the five panel geometries are given in Figure 1 and Tables 1-2. As described in Table 1, Panels 1-2 had forked trailing edges that were bent inwards, having a negative value of θ_2 consistent with the definition of trailing edge sweep angle in Figure 1(b). Panel 3 had a vertical, or straight trailing edge where $\theta_2 = 0°$, and Panels 4-5 had pointed trailing edges that bent outwards, having a positive value of θ_2. Given these geometric definitions, increases in panel number correspond to a more pointed trailing edge. For all five panels, the leading edge sweep angle, θ_1, was held constant at 45°. The Reynolds number in the current work is defined as $Re_c = Uc/\nu$, where c is the chord length of the panel at the midspan and ν is the kinematic viscosity of the water. The aspect ratio of each panel is defined as $AR = b^2/S$, where b is the span taken at the trailing edge and S is the planform area. The range of AR reported in Table 1 agrees well with the observed AR of the caudal fins of multiple biological swimmers (Nursall (1958); Magnuson (1978)). All five panels had the same value of b = 254 mm. The not-to-scale schematic of Figure 1(a) depicts the vertical motion of the traverse motion that was use to collect 27 chordwise-oriented stereoscopic PIV planes for all 25 flow scenarios investigated. With the laser sheet and two overhead PIV cameras mounted in a fixed position, PIV data for a given panel geometry and pitching amplitude was collected at a desired spanwise location at a rate of 4 Hz. At each spanwise location, data was collected at 24 phases of the pitching cycle, with 15 image pairs captured for each individual phase. The resulting instantaneous velocity vectors were then subsequently phase-averaged. Once velocity data was successfully gathered at a given spanwise location, the traverse was used to move the panel vertically through the water tunnel and this data collection process was repeated. The spanwise spacing between PIV planes was constant, being equal to 2.54 mm, or 2% of the span. A volumetric reconstruction of the velocity field in the wake can be obtained by mirroring the data within the 26 planes collected below the symmetry plane about the symmetry plane.

Calculations of positive spanwise circulation, Γ, were performed using the spanwise vorticity fields (ω_z) obtained from phase-averaged velocity data. In order to calculate Γ, the local value of ω_z was integrated over an area contained within all contours of $\omega_z = 1\ s^{-1}$ in accordance with Stokes' circulation theorem. This calculation procedure was similar to that used in previous experimental work (Gharib *et al.* (1998); Buchholz *et al.* (2011); DeVoria & Ringuette (2012)). The total amount of positive spanwise circulation generated during the entire duration of the pitching cycle was tracked as it was shed from the trailing edge and subsequently convected downstream. Only spanwise vorticity located downstream of the trailing edge was used to define the bounds of the circulation calculations. In order to investigate vortex saturation, the circulation contained within the main vortex, as well as the total circulation produced during the entire extent of the pitching cycle, was separately calcu-

Table 1. Definition of geometric and flow parameters for each of the five panel geometries.

Panel	$\theta_1(°)$	$\theta_2(°)$	c (mm)	AR	$Re_c(\times 10^3)$
1	45	-20	27.4	6.7	2.2
2	45	-10	39.3	5.1	3.1
3	45	0	50.5	4.2	4.0
4	45	10	61.7	3.5	4.9
5	45	20	73.6	3.0	5.9

Table 2. Review of $\phi_{\max}$ and and its associated St for each of the five panel geometries.

	St				
$\phi_{\max}$ (°)	Panel 1	Panel 2	Panel 3	Panel 4	Panel 5
5	0.09	0.10	0.11	0.12	0.14
10	0.17	0.20	0.22	0.24	0.27
15	0.25	0.29	0.33	0.36	0.40
20	0.33	0.38	0.43	0.48	0.53
25	0.41	0.47	0.53	0.59	0.66

lated. The main vortex was defined by the region of the closed vorticity contour containing the maximum amount of circulation, which tended to be the contour enclosing the largest area. Saturation is considered to occur when the total circulation produced exceeds the circulation contained within the main vortex, indicating that the main vortex has reached a maximum strength and is no longer accepts additional vorticity created by the panel. The calculations of Γ took place within a domain that was manually selected at each pitching phase so that downstream edge of the domain could move with the wake structures as they convected downstream. The other boundaries of the calculation domain remained fixed, with the upstream boundary touching the trailing edge location when the panel is oriented parallel to the free-stream flow direction. Due to the size of the PIV data window, it was possible for vorticity to leave the transverse edges of the calculation domain for larger values of $\phi_{\max}$.

RESULTS AND CONCLUSIONS

Results showing the time evolution of spanwise circulation in the midspan plane for all five panel geometries at all five angular pitching amplitudes are displayed in Figure 2. Spanwise circulation contained within the main vortex and in the total flow field are shown as functions of the non-dimensional pitching time, t^*, which is defined as $t^* = t/T$. A full pitching cycle has a period of length T, and the period is considered to start at the beginning of the downstroke, i.e. when the panel is at a motion extreme and is beginning to pitch in the clockwise direction. Although the downstroke is the portion of the pitching cycle where the majority of the positive circulation is generated, relatively small amounts of positive circulation are also shed into the wake during the upstroke. Therefore, the time $t^* = 0$ does not neatly correspond to an instant when positive circulation is generated in a flow field free of positive ω_z. However, the beginning of the downstroke is a convenient time to use as the approximate time when spanwise vorticity begins to be shed by the trailing edge. The circulation contained within the main vortex is denoted by Γ_{main} and the total circulation is expressed as Γ_{total}.

The results shown in Figure 2 demonstrate that dimensional spanwise circulation generally increases as the trailing edge geometry becomes more pointed and the chord length at the midspan of the panel becomes larger. This trend is reflected in the observations of the total circulation and the circulation within the main vortex. The most forked trailing edge geometry, i.e. Panel 1, generates the lowest amount of total circulation and weakest main vortices while Panel 5 tends to generate approximately three times the amount of circulation as Panel 1. Furthermore, increases in Strouhal number, i.e. peak-to-peak trailing edge excursion, are associated with greater total production of spanwise circulation and stronger main vortices. Although $\phi_{\max}$ was increased in constant increments of 5°, greater circulation was generated when larger pitching amplitudes were increased, and behavior that was observed regardless of panel geometry. For example, the maximum value of Γ_{total} for Panel 3 grows by approximately 0.002 mm^2/s as St is increased from $St = 0.11$ to $St = 022$. But, the maximum value of Γ_{total} grows by approximately 0.007 mm^2/s when St increases from $St = 0.43$ to $St = 0.53$. Similar results occur with respect to the circulation contained within the main vortex. For a given panel geometry, as pitching amplitude is increased, the larger chord lengths and pitching amplitudes produce greater amounts of local angular acceleration at the trailing edge of the panel, which likely plays a role in the increased production of spanwise circulation. Previous experimental work has also linked increases in circulation to the presence of stronger streamwise pressure gradients on the surface of the panel (Buchholz *et al.* (2011); DeVoria & Ringuette (2012)). The strength of this streamwise pressure gradient is related in part to the low-pressure region associated with the development of the trailing edge vortex; so, additional angular acceleration likely contributes positively to the development of streamwise gradients along the panel. Figure 2 demonstrates that positive circulation is generated almost exclusively during the downstroke portion of the pitching cycle, i.e when $0 \leq t^* \leq 0.5$. A gradual increase in circulation develops during the downstroke for Panel 1 at all St; however, this increase in circulation becomes more dramatic and increasingly nonlinear for the remaining four panel geometries, especially at larger St. The time evolution of Γ for Panels 4-5 at the largest pitching amplitudes after the completion of the downstroke reveals that Γ appears to rise or fall sharply rather than maintain a plateau. This behavior is a spurious result that stems from the manner in which Γ was calculated. As wake structures convect downstream and undergo phenomena such as diffusion, annihilation, and wake breakdown, the isocontours of vorticity used to calculate Γ may interact with those generated during a previous pitching cycle, creating a misleading result for Γ.

Unlike the results of DeVoria & Ringuette (2012) for a trapezoidal panel rotated about its leading edge, there is minimal evidence of vortex saturation for the wakes studied in the current work. As the panel rotates during the downstroke portion of the pitching cycle ($0 \leq t^* \leq 0.5$), vorticity is fed into the wake until the generation of positive vorticity stops and the total circulation attains a peak value. Except for Panel 4 at $St = 0.59$ and Panel 5 at $0.53 \leq St \leq 0.66$, the total circulation tends to closely match the amount of circulation contained within the main spanwise vortex. Vortex saturation would be evidenced by a significantly greater amount of total circulation in comparison to the circulation contained within the boundaries of the main vortex. It is not currently understood why the majority of the flow fields studied in the current work fail to saturate, while prior experiments have produced saturated vortices in similar scenarios (Rival *et al.* (2009); Milano & Gharib (2005); DeVoria & Ringuette (2012)).

Discussions of vortex saturation often focus on a non-dimensional vortex formation number, which is defined as the non-dimensional formation time when the main vortex is no longer able to accept additional vorticity (Gharib *et al.* (1998); Dabiri (2009)). After this formation time occurs, the vortex generator may still continue to create vorticity; however, the vorticity will remain outside the boundary of the main vortex. In previous works, various definitions of the vortex formation time have been used in order to account for the specific details of the vortex generator. The current work uses a definition of the formation time, $\hat{T}$, similar to that employed by Rival *et al.* (2009) in their study of the leading edge vortex vortices produced by a plunging airfoil. $\hat{T}$ is calculated as shown in Equation 1,

$$\hat{T} = \frac{\Gamma}{c\Delta U} \tag{1}$$

In Equation 1, ΔU is a velocity scale that characterizes the shear layer strength. Here, ΔU is taken as the maximum velocity of the trailing edge, $2\pi f c\phi_{\max}$. Using this definition, the maximum formation time for Panels 1-5 was 4.3, 2.8, 2.4, 2.3, and 1.2, respectively. It has been suggested that unsteady vortical flows universally saturate at a formation number of $\hat{T} \approx 4$ Dabiri (2009); so, the lack of saturation in the current work could be due to the relatively low formation times studied.

The results displayed in Figure 2 are restricted to the plane of the midspan, and do not provide a picture of how spanwise circulation varies vertically throughout the wake. In order to investigate the variation of Γ_{total} with respect to spanwise location, z, the vorticity fields were analyzed at $t^* = 0.5$, the time corresponding to the completion of the downstroke. This time was chosen so that the circulation generated by the panel could be discussed prior to significant diffusion and annihilation of vorticity. It was found that vortex structures that were coherent near the midspan plane tended to lose their coherence away from midspan. Accordingly, it was difficult to establish the behaviors of the main vortex as distance from the plane of symmetry increased, and Figure 3 only depicts the values of Γ_{total} with respect to z. All panel geometries produce wakes that contain a region where Γ_{total} is approximately independent of z, and does not vary appreciably with distance away from the midspan plane. In agreement with the results of Figure 2, a panel with a more pointed trailing edge tends to produce greater amounts of circulation in the planes where total circulation is not strongly influenced by spanwise location. For planes closer to the spanwise tips of the panel, Γ_{total} decreases and becomes a function of the spanwise location, ultimately approaching a value near zero in the plane above the tip of the panel. The extent of the region where Γ_{total} is independent of z is influenced by panel geometry and pitching amplitude. The size of this region is larger for panels that are more forked and for pitching amplitudes that are smaller. For example, with respect to Panel 1, Γ_{total} becomes a relatively strong function of z at $z/2b \approx 0.75$ when $St = 0.25$ and at $z/2b \approx 0.65$ when $St = 0.41$. However, these locations decrease for Panel 5, where Γ_{total} becomes a strong function of z at $z/2b \approx 0.65$ when $St = 0.40$ and at $z/2b \approx 0.4$ when $St = 0.66$. A more pointed panel typically generates greater circulation than a more forked panel. Even when both panels pitch with the same kinematics, more circulation is generated at a z location where Γ_{total} is independent of z for the former, but not the latter. For instance, $\Gamma_{\text{total}} \approx 0.01$ mm^2/s at $z/2b = 0.5$ for Panel 1 when $St = 0.41$. But at $z/2b = 0.5$, $\Gamma_{\text{total}} \approx 0.015$ mm^2/s when $St = 0.53$, and $\Gamma_{\text{total}} \approx 0.03$ mm^2/s when $St = 0.66$, for Panel 3 and Panel 5, respectively. Therefore, more forked panels tend to generate less spanwise circulation, even in spanwise regions where the total circulation shed by more pointed panels has decreased from what was generated closer to the midspan.

REFERENCES

Bandyopadhyay, Promode R. 2005 Trends in biorobotic autonomous undersea vehicles. *IEEE Journal of Oceanic Engineering* **30** (1).

Buchholz, James H.J., Green, Melissa A. & Smits, Alexander J. 2011 Scaling the circulation shed by a pitching panel. *J. Fluid Mech.* **688**, 591–601.

Carr, Z.R., Chen, C. & Ringuette, M.J. 2013 Finite-span rotating wings: three-dimensional vortex formation and variations with aspect ratio. *Experiments in Fluids* **54**.

Carr, Zakery R., DeVoria, Adam C. & Ringuette, Matthew J. 2015 Aspect-ratio effects on rotating wings: circulation and forces. *J. Fluid Mech.* **767**, 497–525.

Dabiri, John O. 2009 Optimal vortex formation as a unifying priciple in biological propulsion. *Annu. Rev. Fluid Mech.* **41**, 17–33.

DeVoria, Adam C. & Ringuette, Matthew J. 2012 Vortex formation and saturation for low-aspect-ratio rotating flat-plate fins. *Exp. Fluids* **52**, 441–462.

Fierstine, Harry Lee 1965 Studies in the locomtion and anatomy of scombroid fishes. PhD thesis, University of California Los Angeles.

Gharib, Morteza, Rambod, Edmond & Shariff, Karim 1998 A universal time scale for vortex ring formation. *J. Fluid Mech.* **360**, 121–140.

Lauder, George V. 2000 Function of the caudal fin during locomotion in fishes: Kinematics, flow visualization, and evolutionary patterns. *Integrative and Comparative Biology* **40** (1), 101–122.

Lighthill, M.J. 1969 Hydromechanics of aquatic animal propulsion. *Ann. Rev. Fluid Mech.* **1**, 413–446.

Magnuson, John J. 1978 *Fish Physiology Volume VII Locomotion*, chap. Locomotion by Scombrid Fishes: Hydromechanics, Morphology, and Behavior, pp. 239–313. Academic Press.

Milano, Michele & Gharib, Morteza 2005 Uncovering the physics of flapping flat plates with artificial evolution. *J. Fluid Mech.* **534**, 403–409.

Nursall, J.R. 1958 The caudal fin as a hyrdofoil. *Evolution* **12** (1), 116–120.

Rival, David, Prangemeier, Tim & Tropea, Cameron 2009 The influence of airfoil kinematics on the formation of leading-edge vortices in bio-inspired flight. *Exp. Fluids* **46**.

Shang, J. K., Combes, S.A., Finio, B.M. & Wood, R.J. 2009 Artificial insect wings of diverse morphology for flapping-wing micro air vehicles. *Bioinspiration & Biomimetics* **4** (3).

Triantafyllou, G.S., Triantafyllou, M.S. & Grosenbaugh, M.A. 1993 Optimal thrust development in oscillating foils with application to fish propulsion. *Journal of Fluids and Structures* **7**, 205–224.

Triantafyllou, Michael S., Techet, Alexandra H. & Hover, Franz S. 2004 Review of experimental work in biomimetic foils. *IEEE Journal of Oceanic Engineering* **29** (3), 585–594.

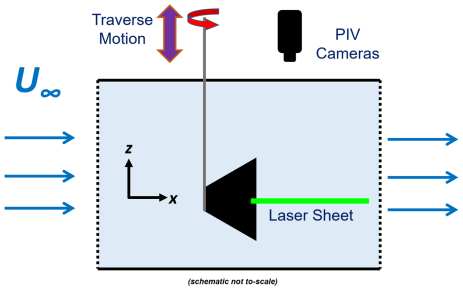

(a) Schematic showing the pitching panel, laser sheet, PIV cameras, traverse motion, direction of the free-stream flow, and coordinate definitions.

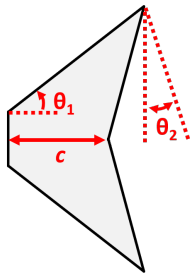

(b) Schematic showing variables that define panel geometries.

Figure 1. Schematics detailing experimental setup of water tunnel and definitions used for panel geometries.

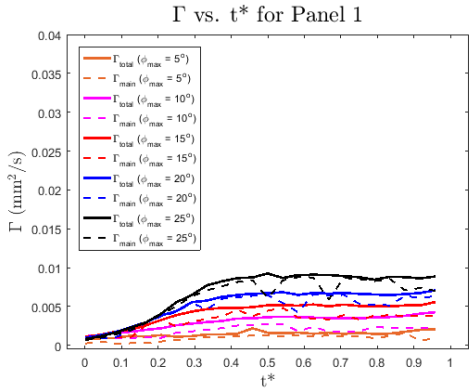

(a) Total circulation and main vortex circulation as a function of non-dimensional time for Panel 1.

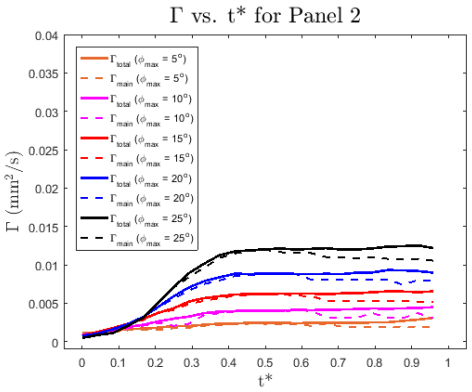

(b) Total circulation and main vortex circulation as a function of non-dimensional time for Panel 2.

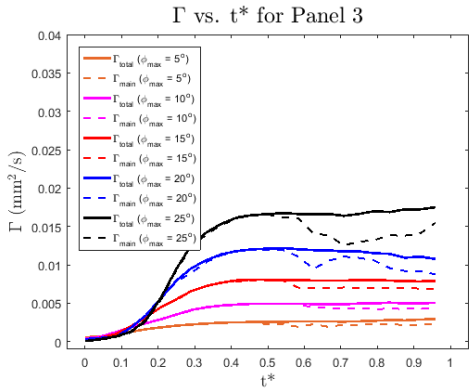

(c) Total circulation and main vortex circulation as a function of non-dimensional time for Panel 3.

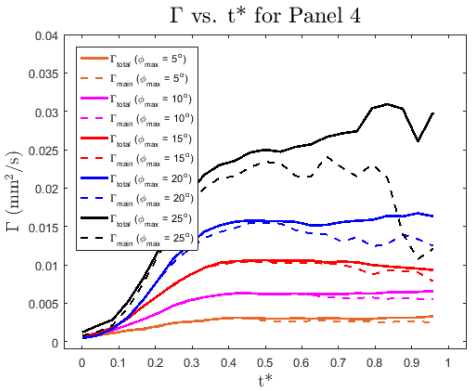

(d) Total circulation and main vortex circulation as a function of non-dimensional time for Panel 4.

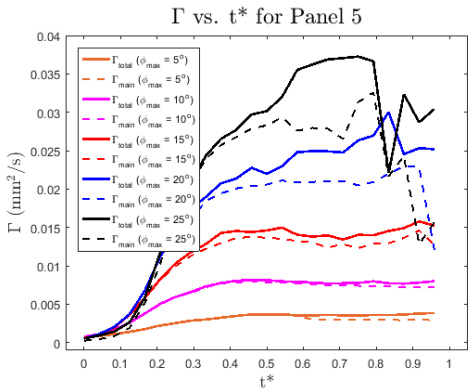

(e) Total circulation and main vortex circulation as a function of non-dimensional time for Panel 5.

Figure 2. Total circulation and main vortex circulation as a function of non-dimensional time for all five panel geometries.

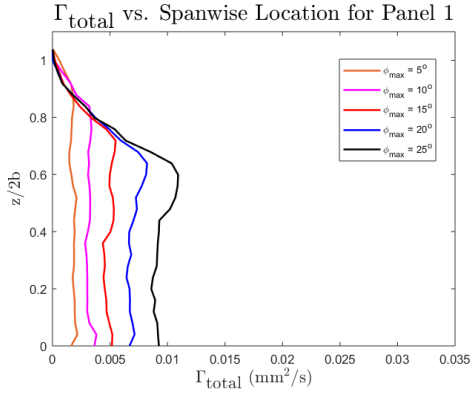

(a) Total circulation as a function of spanwise location for Panel 1.

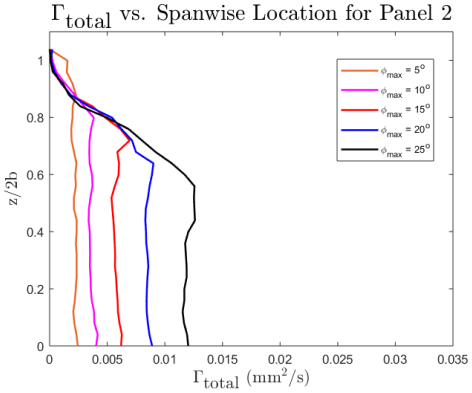

(b) Total circulation as a function of spanwise location for Panel 2.

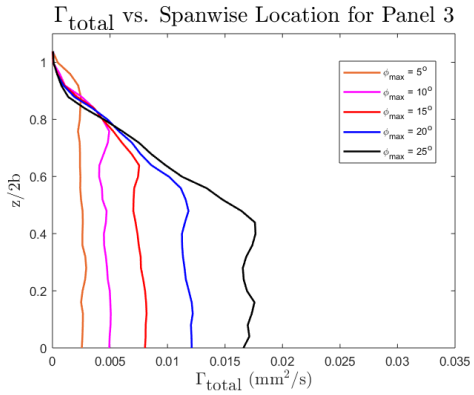

(c) Total circulation as a function of spanwise location for Panel 3.

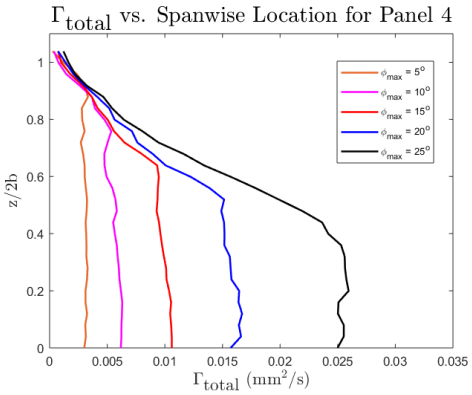

(d) Total circulation as a function of spanwise location for Panel 4.

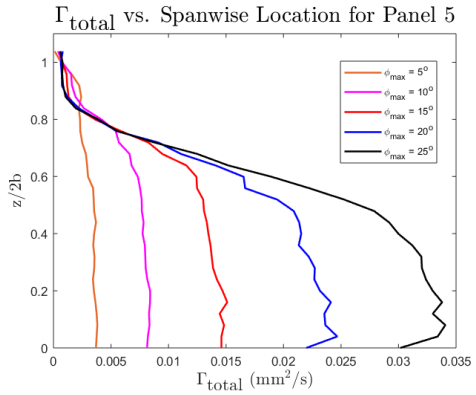

(e) Total circulation as a function of spanwise location for Panel 5.

Figure 3. Total circulation as a function of spanwise location for all five panel geometries.